Chemistry–A European Journal

Supporting Information

Organometallic Platinum(II) Photosensitisers that Demonstrate Ligand-Modulated Triplet-Triplet Annihilation Energy Upconversion Efficiencies

Sophie A. Fitzgerald, Xiao Xiao, Jianzhang Zhao,* Peter N. Horton, Simon J. Coles, Richard C. Knighton, Benjamin D. Ward, and Simon J. A. Pope*

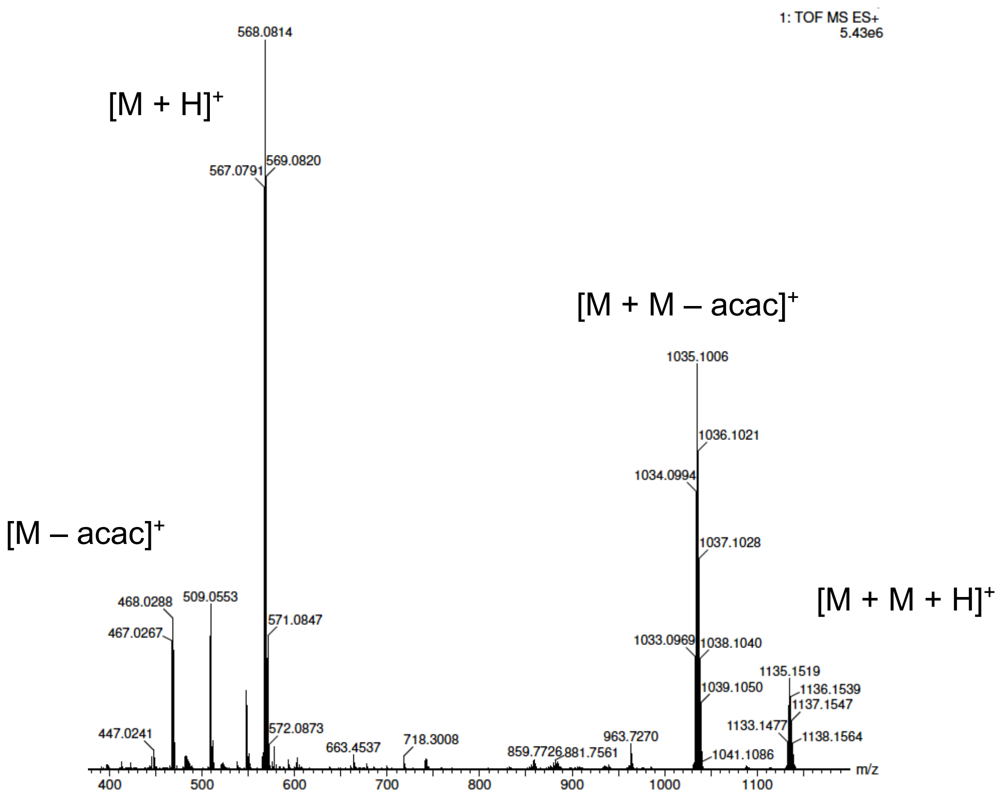

Figure S1. Example of a HRMS spectrum for [Pt(**L⁴**)(acac)].

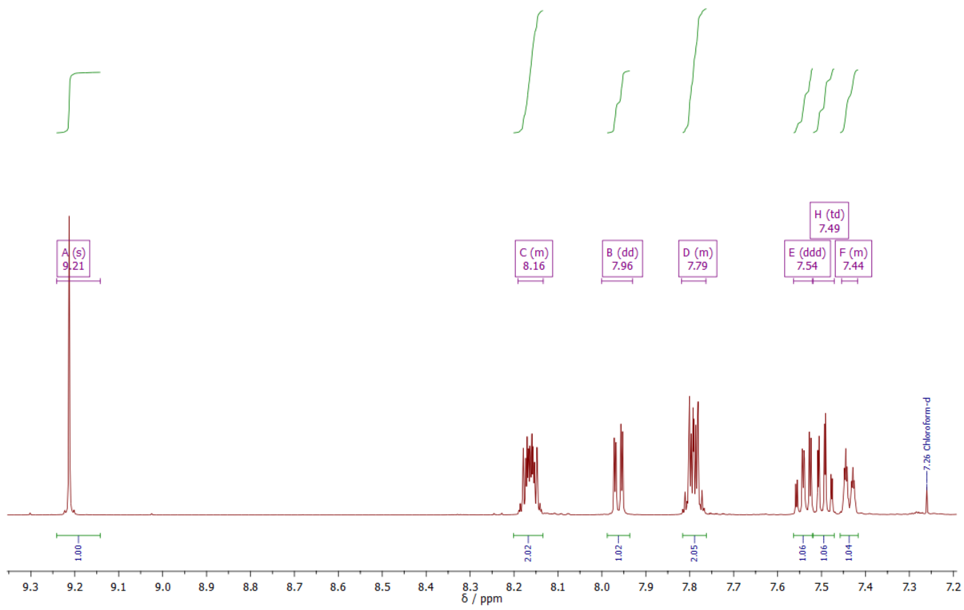

Figure S2. ^{1}H NMR spectrum for H**L¹** (500 MHz, $CDCl_3$).

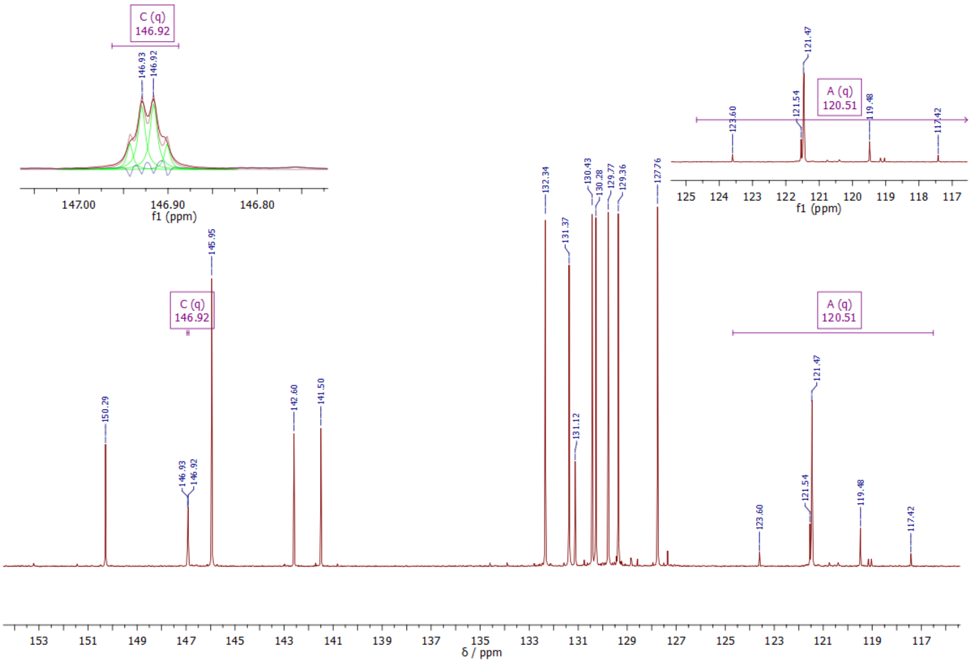

Figure S3. $^{13}C\{^{1}H\}$ NMR spectrum for H**L**^{1} (126 MHz, $CDCl_3$).

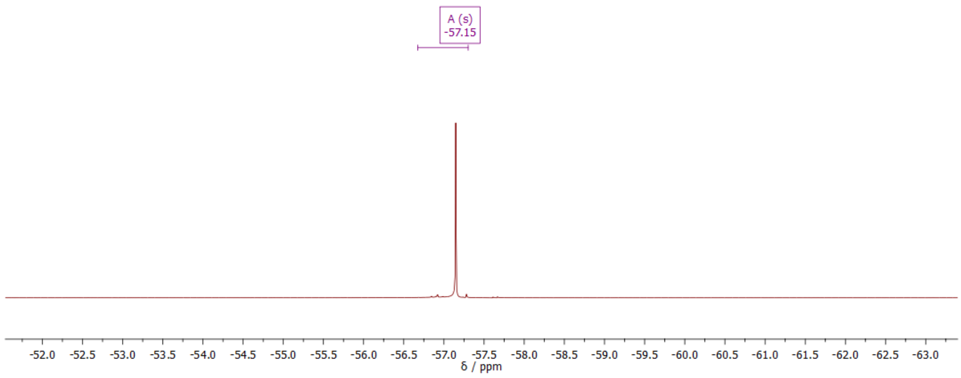

Figure S4. $^{19}F\{^{1}H\}$ NMR spectrum for H**L**^{1} (376 MHz, $CDCl_3$).

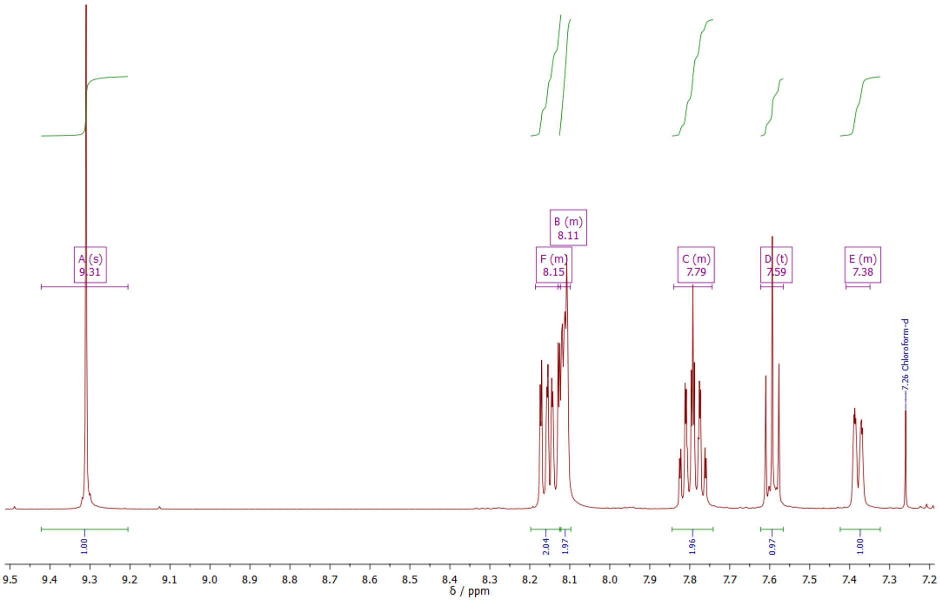

Figure S5. ^{1}H NMR spectrum for H**L²** (500 MHz, $CDCl_3$).

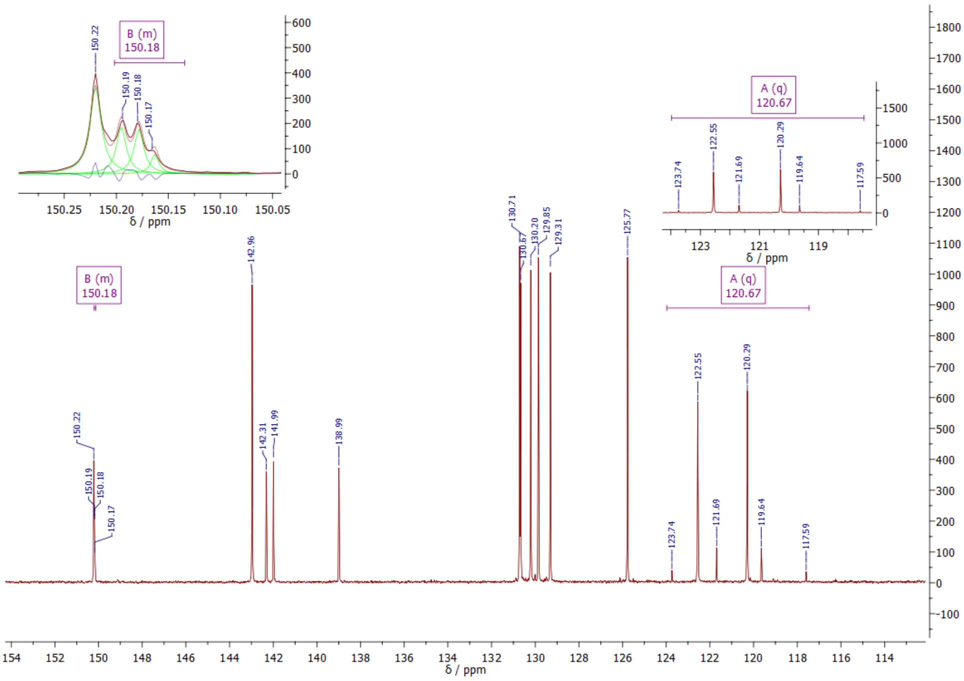

Figure S6. $^{13}C\{^{1}H\}$ NMR spectrum for H**L²** (126 MHz, $CDCl_3$).

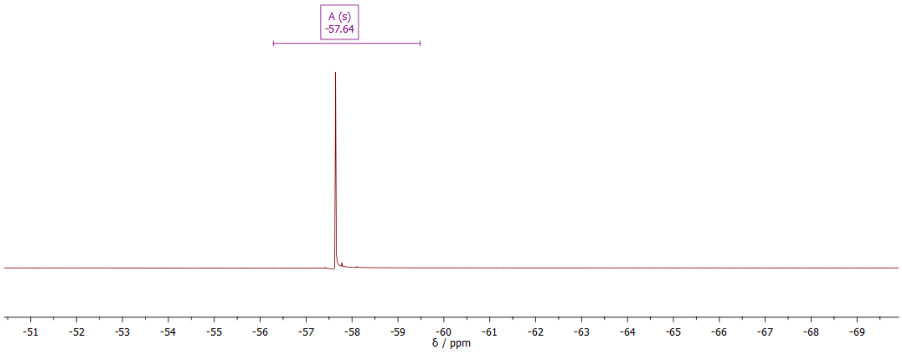

Figure S7. $^{19}F\{^{1}H\}$ NMR spectrum for H**L**$^{\mathbf{2}}$ (376 MHz, $CDCl_3$).

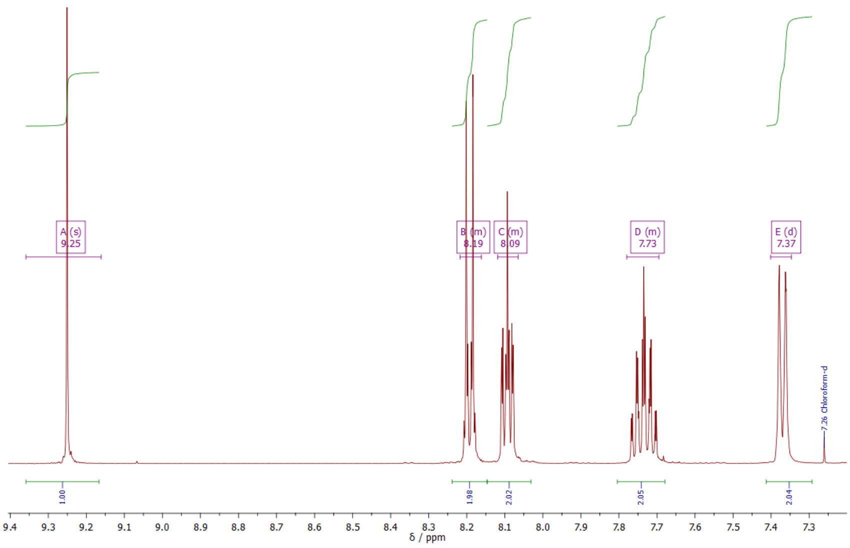

Figure S8. ^{1}H NMR spectrum for H**L**$^{\mathbf{3}}$ (500 MHz, $CDCl_3$).

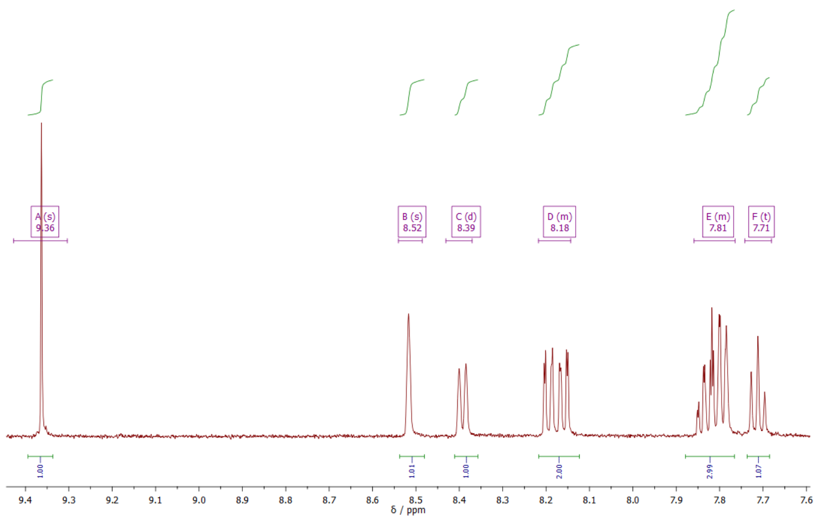

Figure S9. ^{1}H NMR spectrum for H**L**$^{\mathbf{4}}$ (500 MHz, $CDCl_3$).

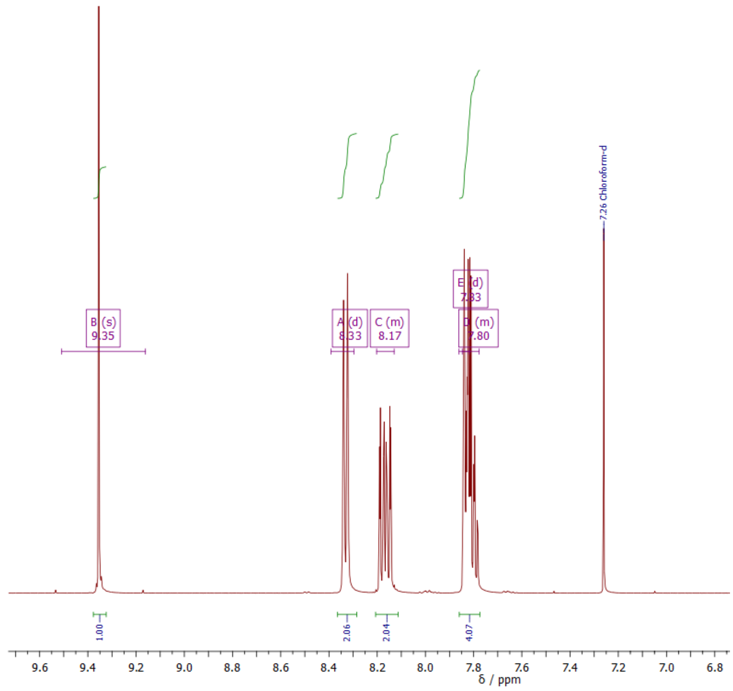

Figure S10. [1]H NMR spectrum for H**L[5]** (500 MHz, $CDCl_3$).

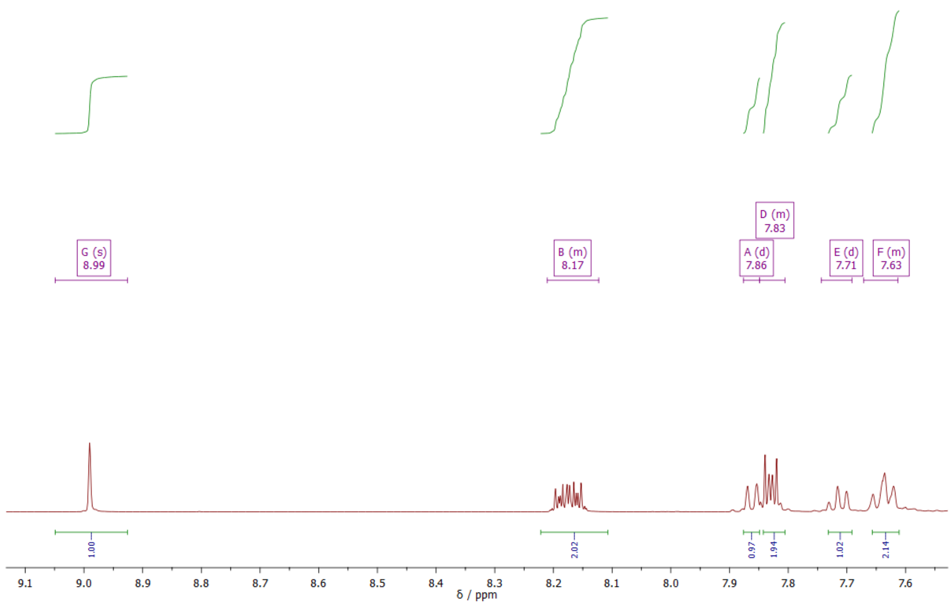

Figure S11. [1]H NMR spectrum for H**L[6]** (500 MHz, $CDCl_3$).

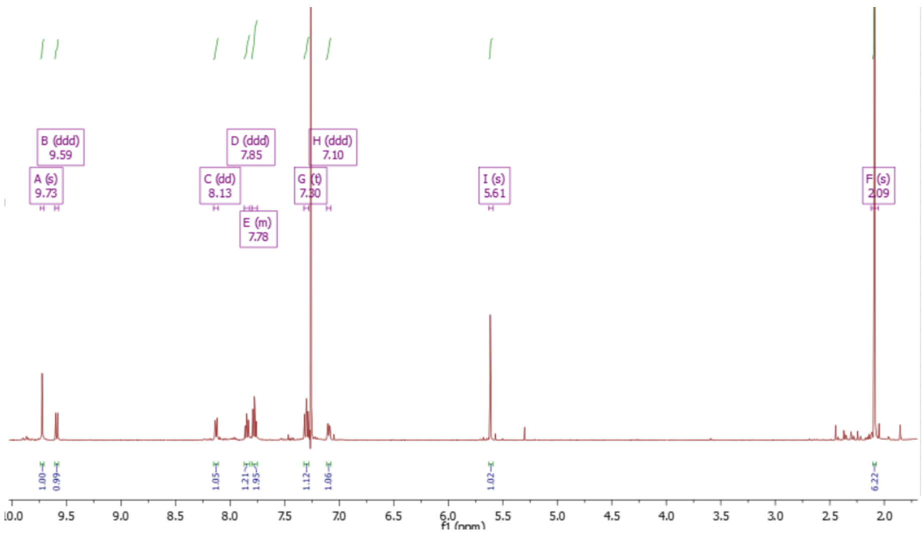

Figure S12. ^{1}H NMR spectrum for [Pt(**L^{1}**)(acac)] (500 MHz, $CDCl_3$).

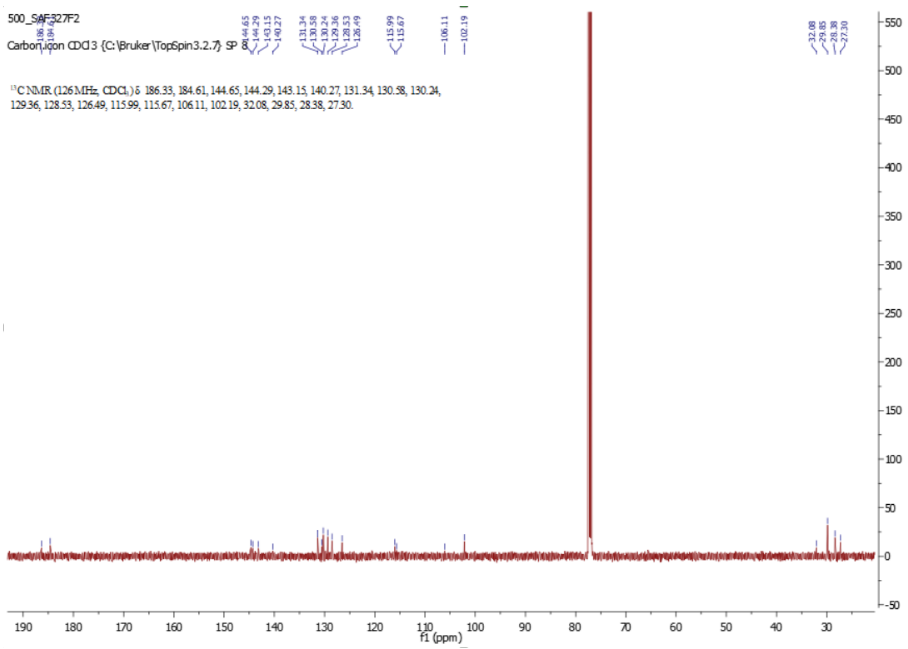

Figure S13. $^{13}C\{^{1}H\}$ NMR spectrum for [Pt(**L^{1}**)(acac)] (126 MHz, $CDCl_3$).

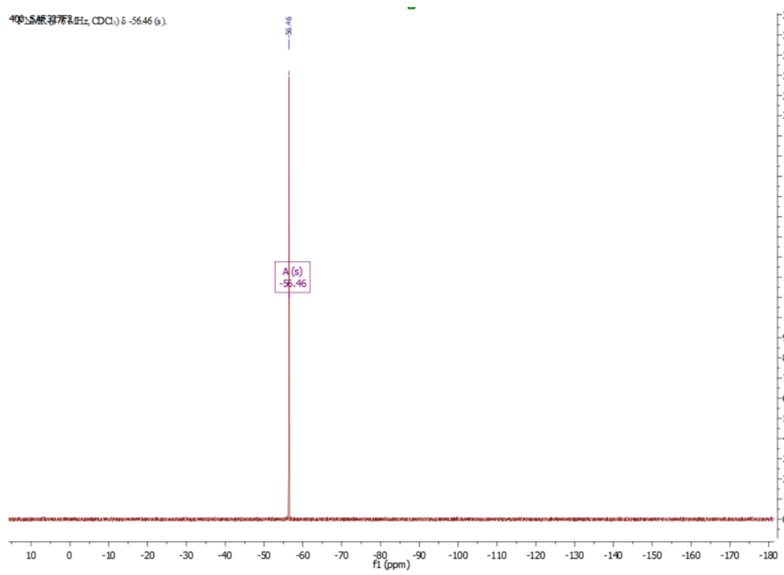

Figure S14. $^{19}F\{^{1}H\}$ NMR spectrum for [Pt(**L¹**)(acac)] (376 MHz, $CDCl_3$).

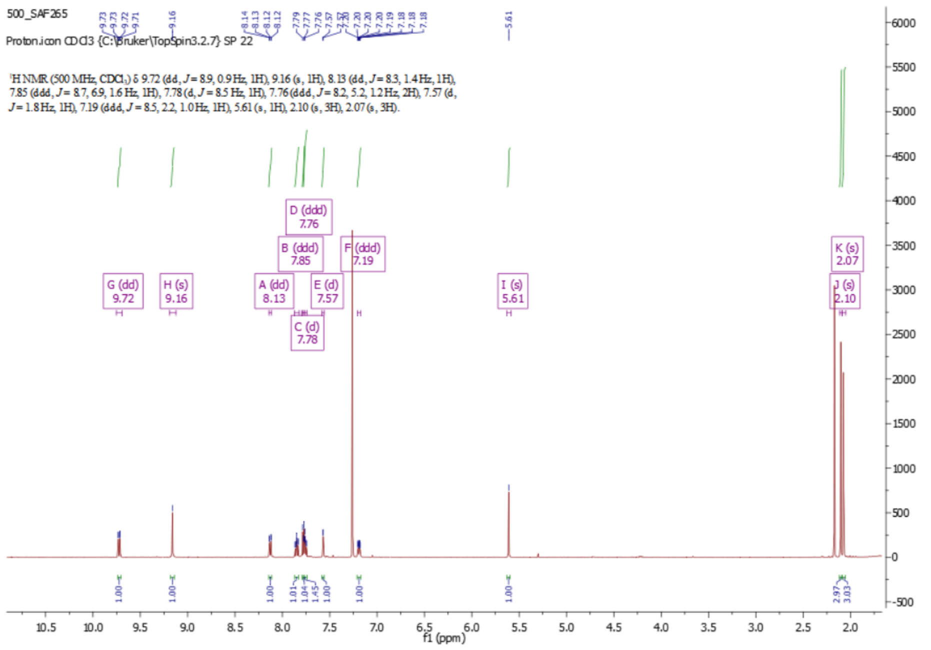

Figure S15. ^{1}H NMR spectrum for [Pt(**L²**)(acac)] (500 MHz, $CDCl_3$).

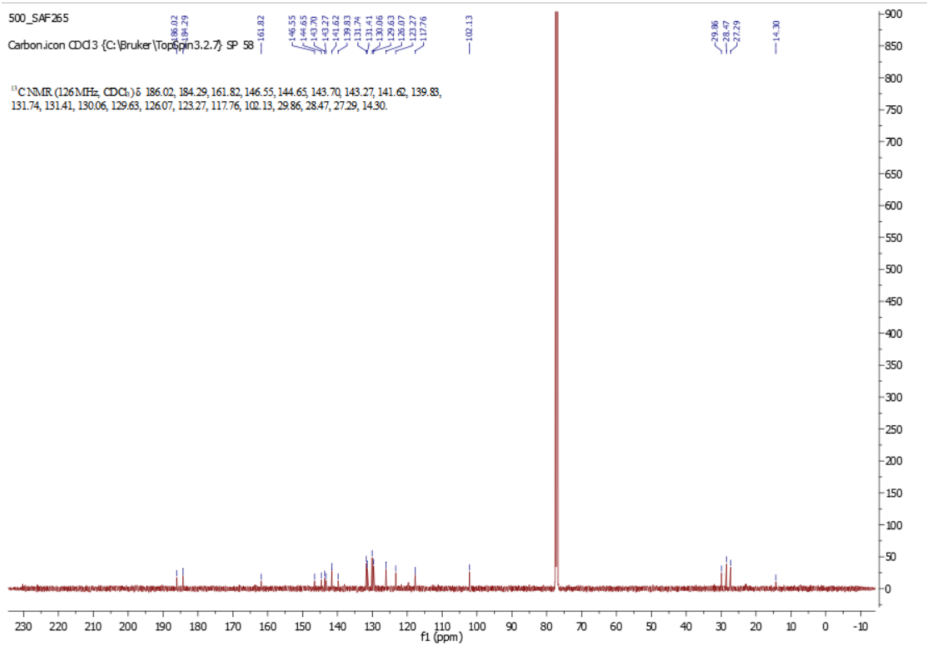

Figure S16. $^{13}C\{^{1}H\}$ NMR spectrum for [Pt(**L²**)(acac)] (126 MHz, $CDCl_3$).

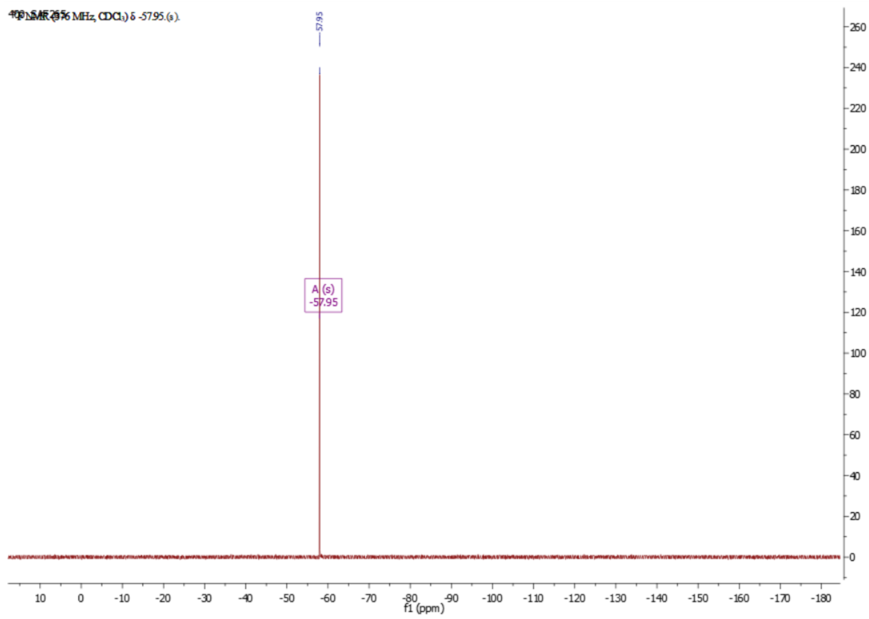

Figure S17. $^{19}F\{^{1}H\}$ NMR spectrum for [Pt(**L²**)(acac)] (376 MHz, $CDCl_3$).

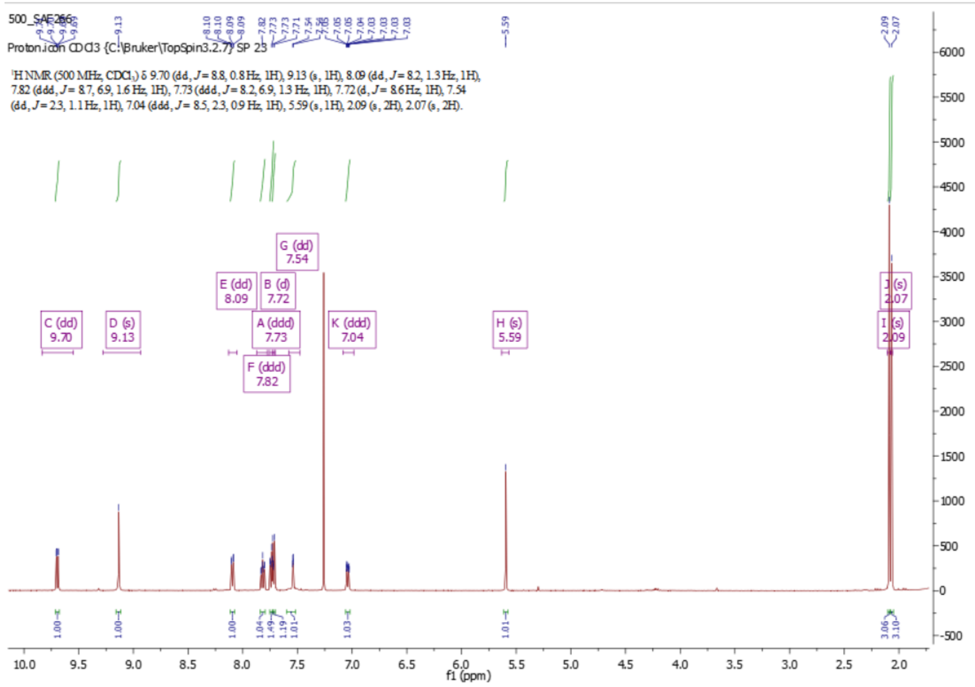

Figure S18. ^{1}H NMR spectrum for [Pt(**L**^{3})(acac)] (500 MHz, $CDCl_3$).

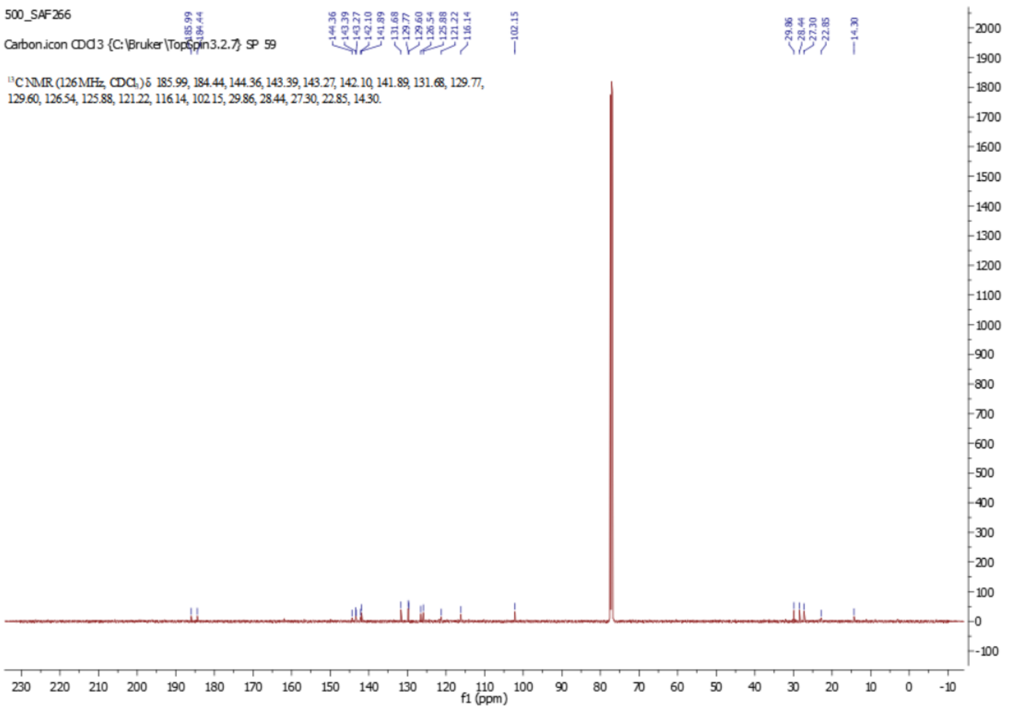

Figure S19. ^{13}C{^{1}H} NMR spectrum for [Pt(**L**^{3})(acac)] (126 MHz, $CDCl_3$).

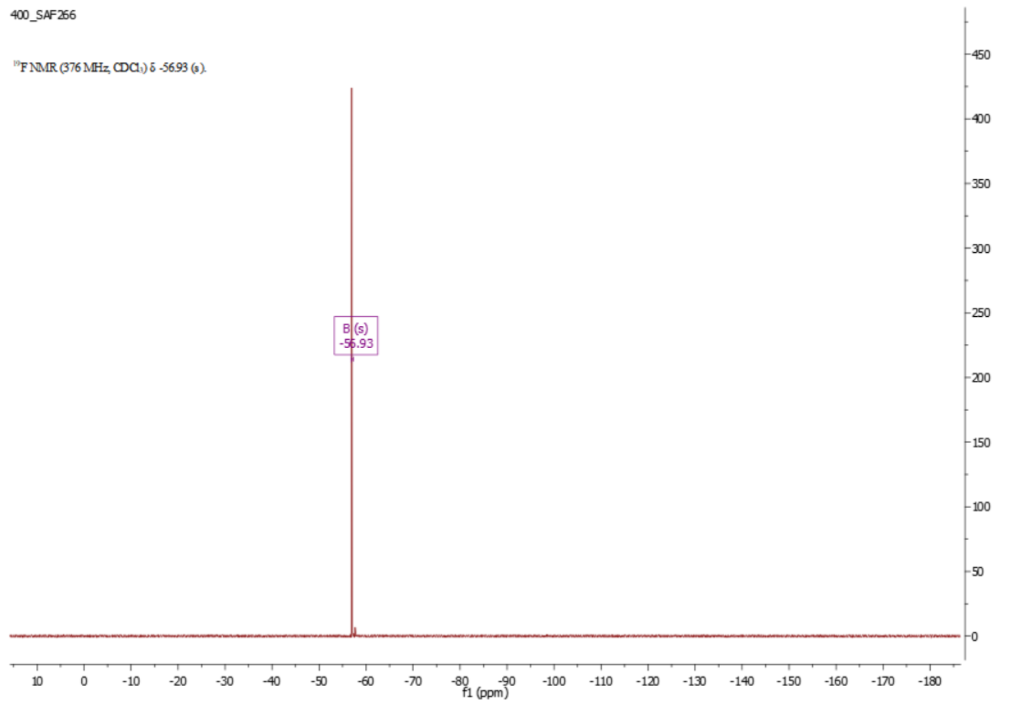

Figure S20. $^{19}F\{^{1}H\}$ NMR spectrum for [Pt(**L^3**)(acac)] (376 MHz, $CDCl_3$).

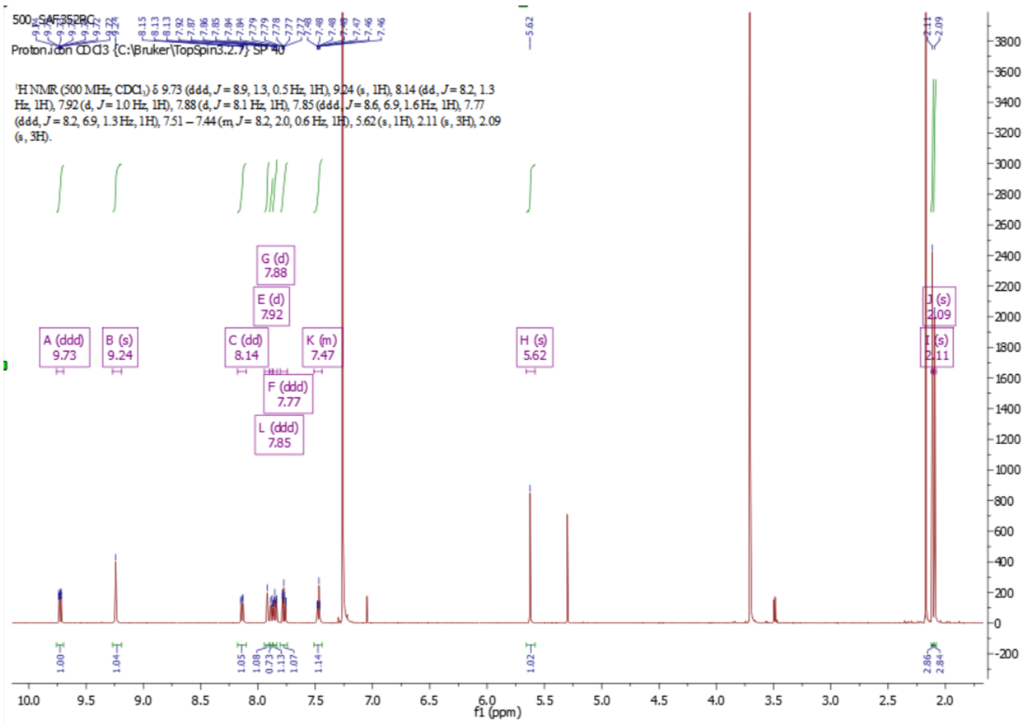

Figure S21. ^{1}H NMR spectrum for [Pt(**L^4**)(acac)] (500 MHz, $CDCl_3$).

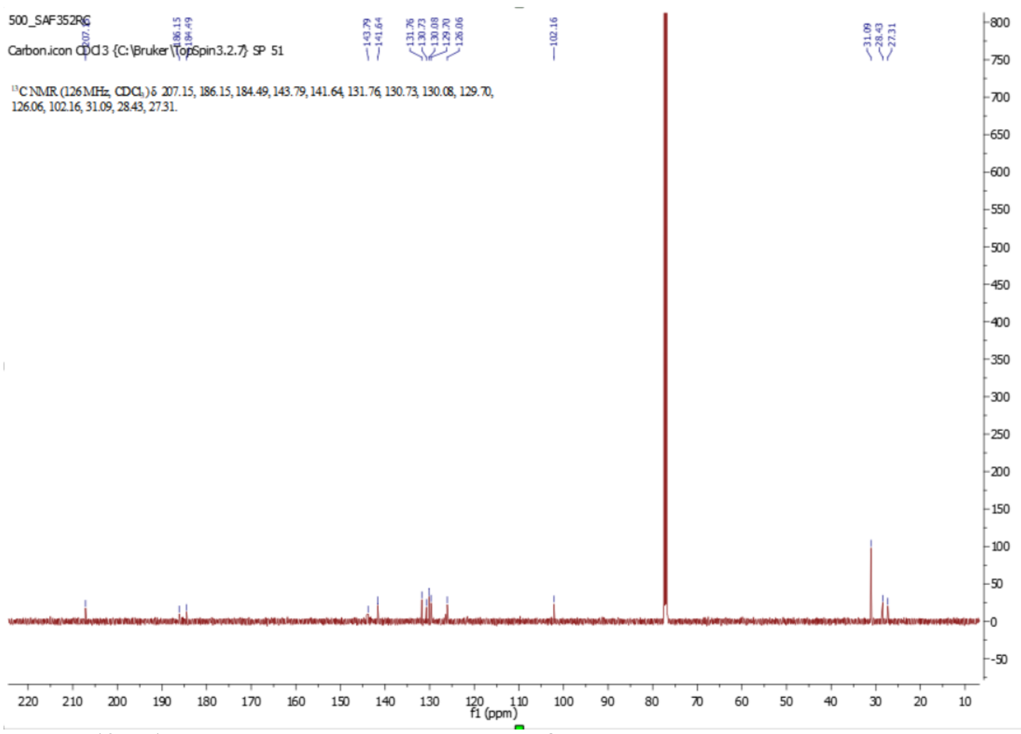

Figure S22. $^{13}C\{^{1}H\}$ NMR spectrum for [Pt(**L⁴**)(acac)] (126 MHz, $CDCl_3$).

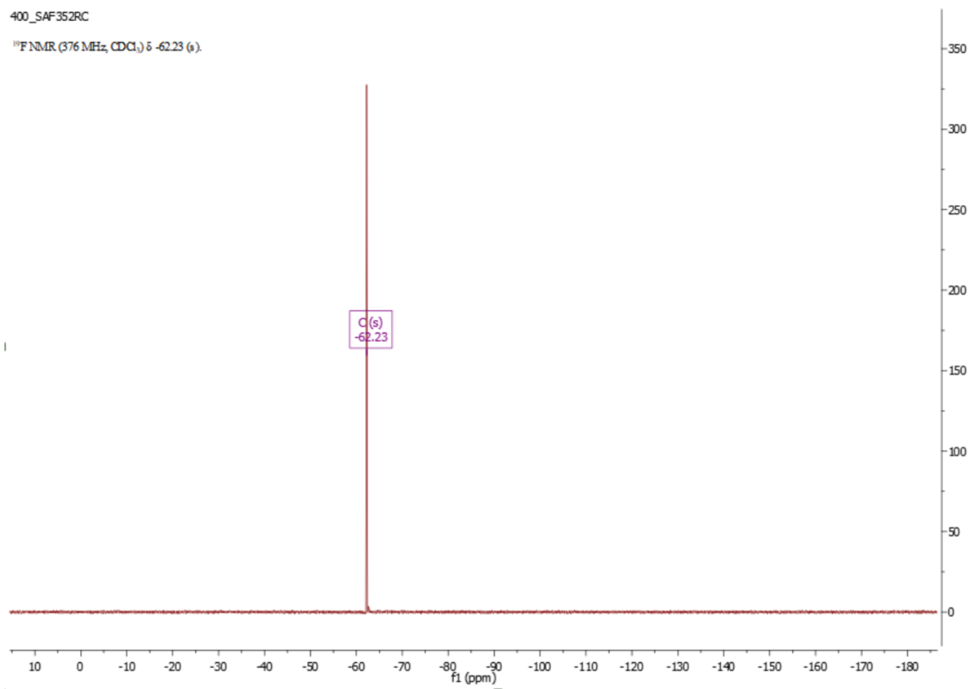

Figure S23. $^{19}F\{^{1}H\}$ NMR spectrum for [Pt(**L⁴**)(acac)] (376 MHz, $CDCl_3$).

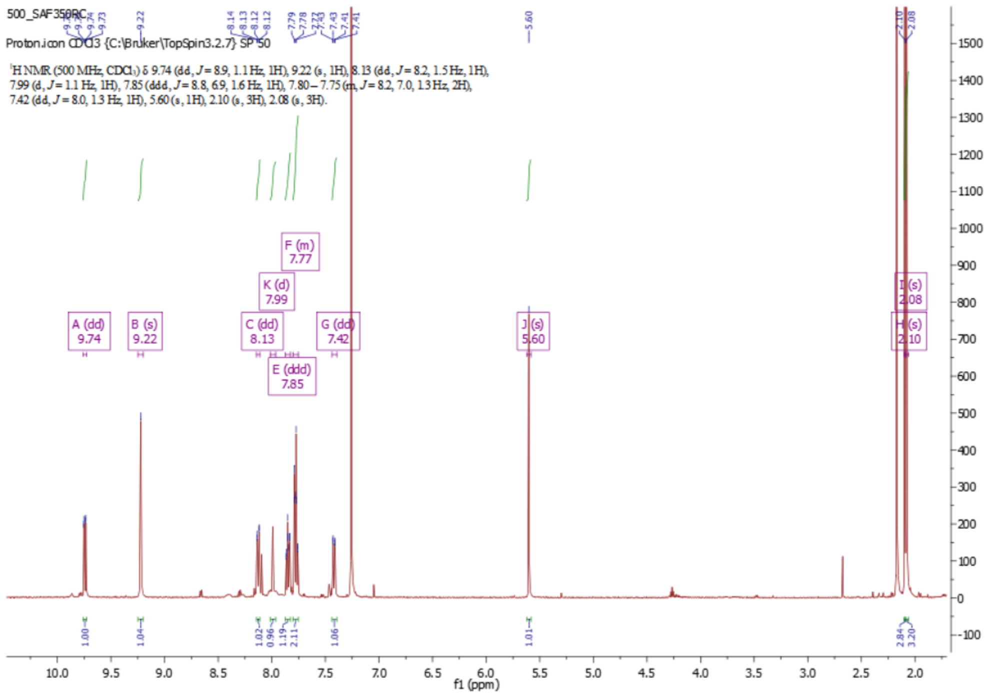

Figure S24. ^{1}H NMR spectrum for [Pt(**L⁵**)(acac)] (500 MHz, $CDCl_3$).

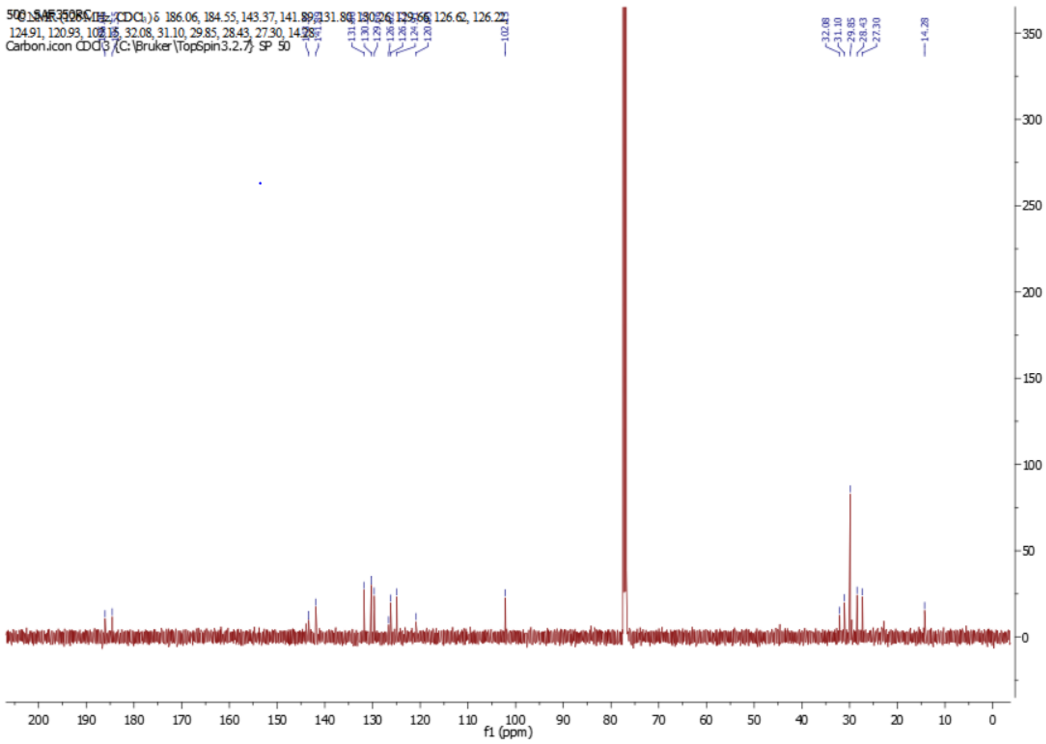

Figure S25. $^{13}C\{^{1}H\}$ NMR spectrum for [Pt(**L⁵**)(acac)] (126 MHz, $CDCl_3$).

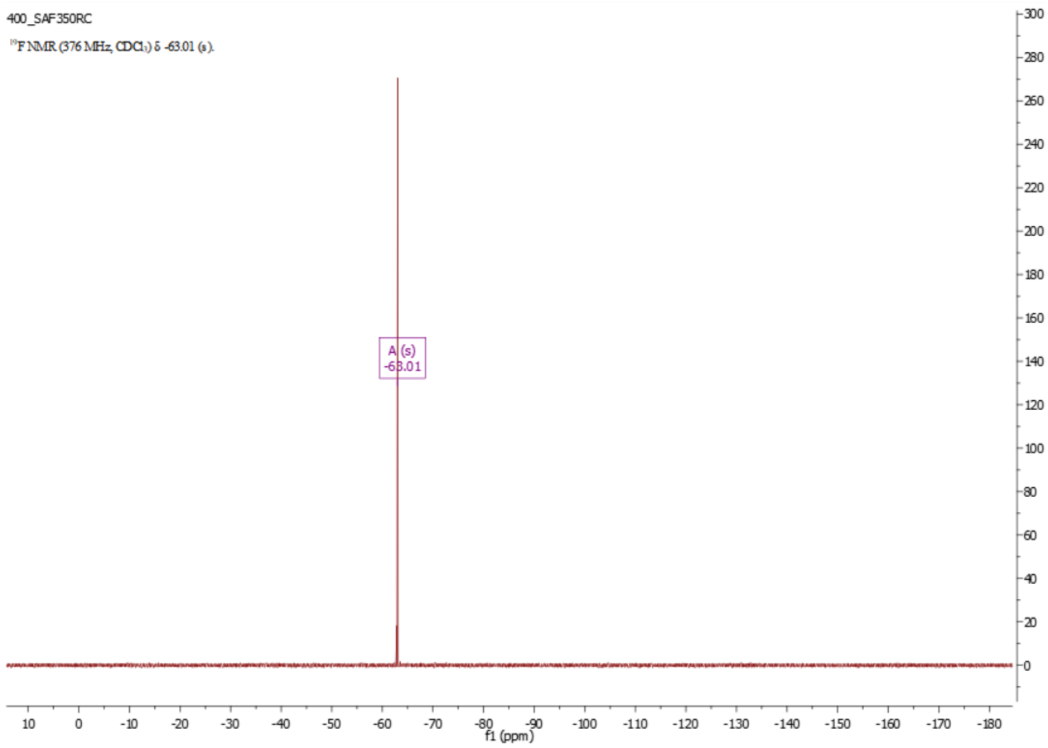

Figure S26. $^{19}F\{^{1}H\}$ NMR spectrum for [Pt(**L⁵**)(acac)] (376 MHz, $CDCl_3$).

Table S1. Data collection parameters for the X-ray crystallography.

Compound	**[Pt(L¹)(acac)]**	**[Pt(L²)(acac)] 200K**	**[Pt(L²)(acac)] 100K**	**[Pt(L³)(acac)]**
Formula	$C_{20}H_{15}F_3N_2O_3Pt$	$C_{20}H_{15}F_3N_2O_3Pt$	$C_{20}H_{15}F_3N_2O_3Pt$	$C_{20.17}Cl_{0.5}F_3H_{15.17}N_2O_3Pt$
$D_{calc.}$/ g cm^{-3}	2.112	2.076	2.114	2.113
μ/mm^{-1}	14.812	7.572	7.709	7.525
Formula Weight	583.43	583.43	583.43	603.37
Colour	red	red	red	red
Shape	blade-shaped	lath-shaped	needle-shaped	block-shaped
Size/mm^3	0.120×0.050×0.010	0.12×0.08×0.01	0.233×0.034×0.019	0.090×0.080×0.060
T/K	100.0(2)	200(2)	100(2)	100(2)
Crystal System	triclinic	triclinic	triclinic	trigonal
Space Group	*P*-1	*P*-1	*P*-1	*R*-3
a/Å	7.7283(2)	7.6623(2)	7.5818(3)	28.9387(2)
b/Å	11.4387(3)	10.5373(3)	10.4772(4)	28.9387(2)
c/Å	11.5572(3)	12.3368(2)	12.3791(4)	11.76590(10)
α/°	69.743(2)	90.245(2)	91.366(3)	90
β/°	73.859(2)	104.817(2)	106.216(3)	90
γ/°	88.704(2)	103.738(2)	102.858(3)	120
V/Å^3	917.62(4)	933.16(4)	916.66(6)	8533.23(14)
Z	2	2	2	18
Z'	1	1	1	1
Wavelength/Å	1.54178	0.71075	0.71075	0.71075
Radiation type	Cu K_α	Mo K_α	Mo K_α	Mo K_α
Θ_{min}/°	4.771	1.712	2.002	2.375
Θ_{max}/°	68.274	28.700	28.697	30.504
Measured Refl's.	11962	21485	22148	160283
Indep't Refl's	11962	4830	4717	5801
Refl's I≥2 σ(I)	11572	4433	4312	5596
R_{int}	.	0.0631	0.0460	0.0284
Parameters	265	301	301	264
Restraints	0	226	184	0
Largest Peak	3.752	2.379	3.696	1.490
Deepest Hole	-1.010	-1.972	-2.555	-1.287
GooF	1.056	1.045	1.033	1.245
wR_2 (all data)	0.1028	0.0753	0.0708	0.0500
wR_2	0.1021	0.0743	0.0691	0.0496
R_1 (all data)	0.0396	0.0329	0.0369	0.0227
R_1	0.0386	0.0293	0.0311	0.0214

Table S2. Bond lengths (Å) for the crystal structures.

[Pt($\mathbf{L}^1$)(acac)]

Pt1	Pt1[1]	3.2041(6)
Pt1	O21	2.000(5)
Pt1	O22	2.108(5)
Pt1	N1	2.041(6)
Pt1	C1	1.967(8)

[Pt($\mathbf{L}^3$)(acac)]

Pt1	Pt1[1]	3.2586(2)
Pt1	O21	2.094(2)
Pt1	O22	1.994(2)
Pt1	N1	2.044(2)
Pt1	C1	1.965(3)

[Pt($\mathbf{L}^2$)(acac)] 200K

Pt1	Pt1[1]	3.2199(3)
Pt1	O21	1.996(3)
Pt1	O22	2.103(3)
Pt1	N1	2.034(3)
Pt1	C1	1.967(4)

[Pt($\mathbf{L}^2$)(acac)] 100K

Pt1	Pt1[1]	3.2020(3)
Pt1	O21	1.994(3)
Pt1	O22	2.104(3)
Pt1	N1	2.044(4)
Pt1	C1	1.973(4)

Table S3. Bond angles (°) for the crystal structures.

[Pt($\mathbf{L}^1$)(acac)]

O21	Pt1	Pt1[1]	86.48(16)
O21	Pt1	O22	88.4(2)
O21	Pt1	N1	169.9(2)
O22	Pt1	Pt1[1]	81.10(15)
N1	Pt1	Pt1[1]	98.49(18)
N1	Pt1	O22	101.1(2)
C1	Pt1	Pt1[1]	105.1(2)
C1	Pt1	O21	89.7(3)
C1	Pt1	O22	173.4(2)
C1	Pt1	N1	80.5(3)

[Pt($\mathbf{L}^3$)(acac)]

O22	Pt1	O21	89.19(8)
O22	Pt1	N1	169.27(9)
N1	Pt1	O21	100.39(9)
C1	Pt1	O21	175.94(9)
C1	Pt1	O22	88.96(10)
C1	Pt1	N1	81.16(10)

[Pt($\mathbf{L}^2$)(acac)] 200K

O21	Pt1	Pt1[1]	90.16(9)
O21	Pt1	O22	88.71(12)
O21	Pt1	N1	170.10(12)
O22	Pt1	Pt1[1]	83.48(8)
N1	Pt1	Pt1[1]	93.62(9)
N1	Pt1	O22	100.80(13)
C1	Pt1	Pt1[1]	102.22(11)
C1	Pt1	O21	89.38(16)
C1	Pt1	O22	174.00(12)
C1	Pt1	N1	80.88(15)

[Pt($\mathbf{L}^2$)(acac)] 100K

O21	Pt1	Pt1[1]	88.83(9)
O21	Pt1	O22	88.97(13)
O21	Pt1	N1	169.96(14)
O22	Pt1	Pt1[1]	83.01(9)
N1	Pt1	Pt1[1]	94.90(10)
N1	Pt1	O22	100.71(14)
C1	Pt1	Pt1[1]	102.97(12)
C1	Pt1	O21	89.05(17)
C1	Pt1	O22	173.67(15)
C1	Pt1	N1	81.04(17)

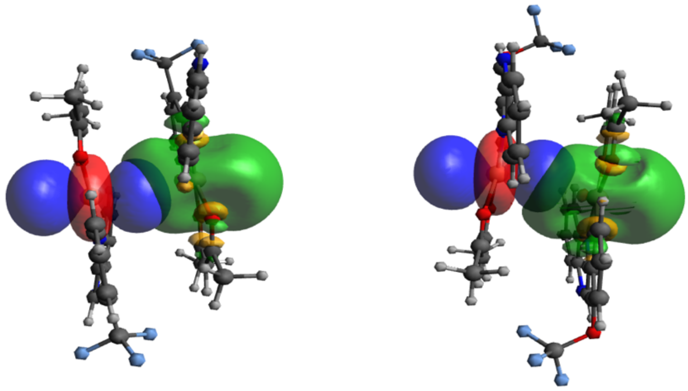

Figure S27. Pictorial description of the natural bonding orbital (NBO) analyses of the interaction between the two Pt atoms of [Pt(**L**[1])(acac)] (left) and [Pt(**L**[2])(acac)].

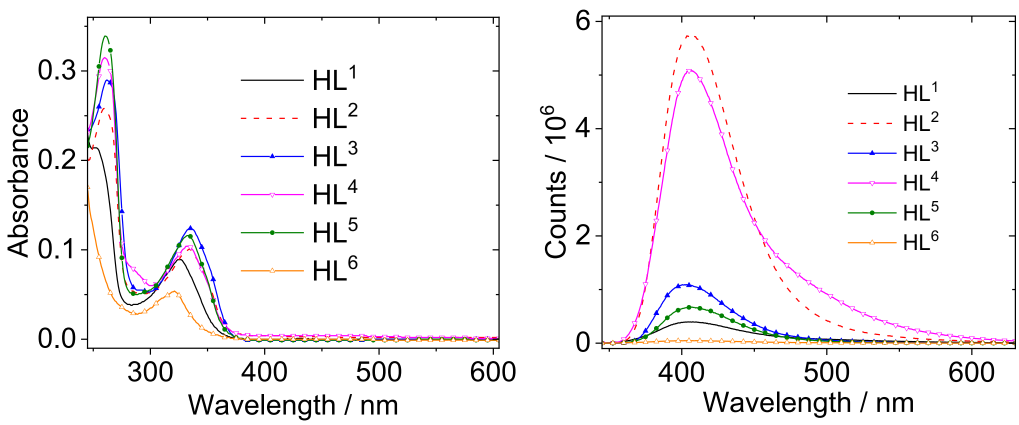

Figure S28. UV-vis. spectra of the ligands (*left*) and corresponding steady state emission spectra (*right*). All using 10^{-5} M $CHCl_3$ solutions.

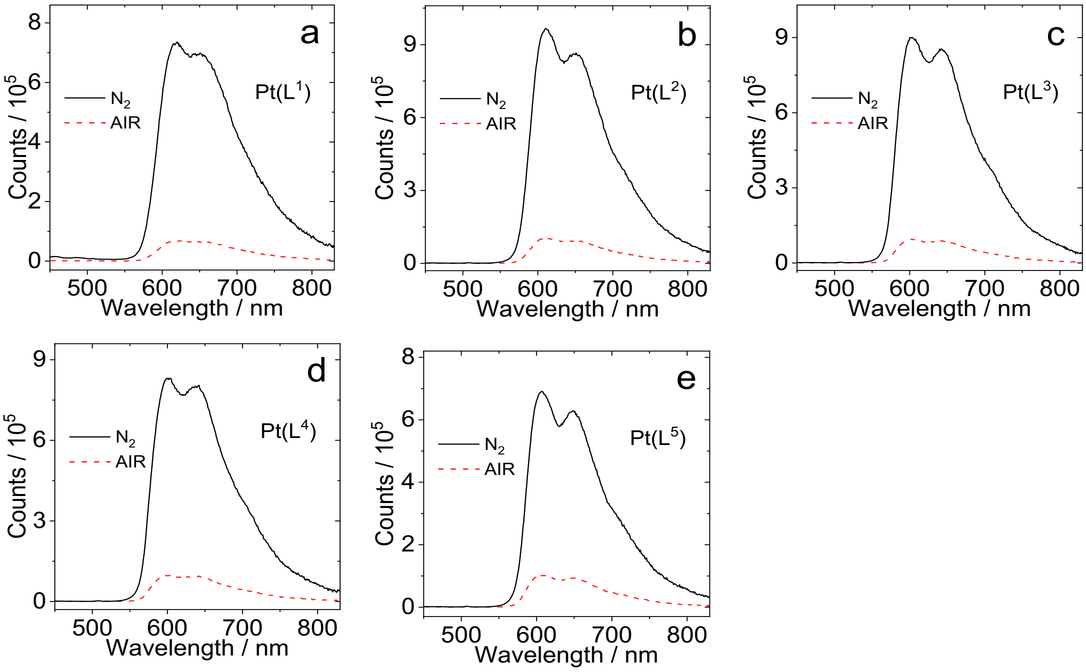

Figure S29. Phosphorescence emission spectra of (a) [Pt(**L^1**)(acac)], (b) [Pt(**L^2**)(acac)], (c) [Pt(**L^3**)(acac)], (d) [Pt(**L^4**)(acac)] and (e) [Pt(**L^5**)(acac)] in *deoxygenated* and *aerated* toluene solution. Optically matched solutions were used (all the solution show the same absorbance at the excitation wavelength, λ_{ex} = 440 nm, $A_{440\ nm}$ = 0.1). 25 °C.

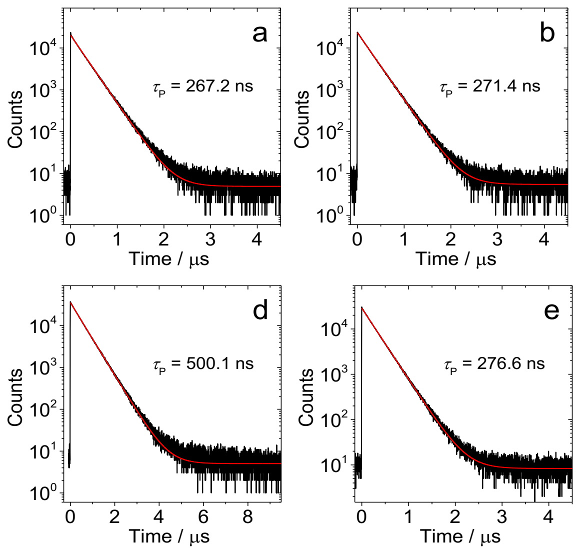

Figure S30. Phosphorescence decay traces of (a) [Pt(**L**[1])(acac)], (b) [Pt(**L**[2])(acac)], (c) [Pt(**L**[3])(acac)], (d) [Pt(**L**[4])(acac)] and (e) [Pt(**L**[5])(acac)] at 750 nm in aerated toluene. λ_{ex} = 405 nm, $A_{405\ nm}$ = 0.1, 25 °C.

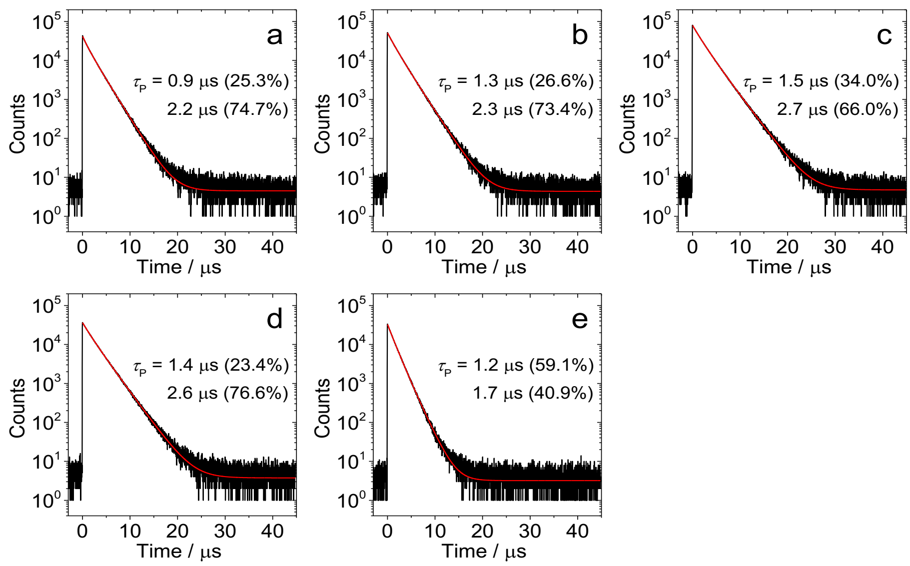

Figure S31. Phosphorescence decay traces of (a) [Pt(**L**[1])(acac)], (b) [Pt(**L**[2])(acac)], (c) [Pt(**L**[3])(acac)], (d) [Pt(**L**[4])(acac)] and (e) [Pt(**L**[5])(acac)] at 750 nm in deoxygenated toluene. λ_{ex} = 405 nm, $A_{405\ nm}$ = 0.1, 25 °C.

Figure S32. Left: Steady state spectra (λ_{ex} = 550 nm) recorded in the solid state for [Pt(**L**^{2})(acac] (blue) and [Pt(**L**^{5})(acac] (green). Right: Photographs of crystalline [Pt(**L**^{2})(acac] under ambient light (left) and UV irradiation (right)**.**

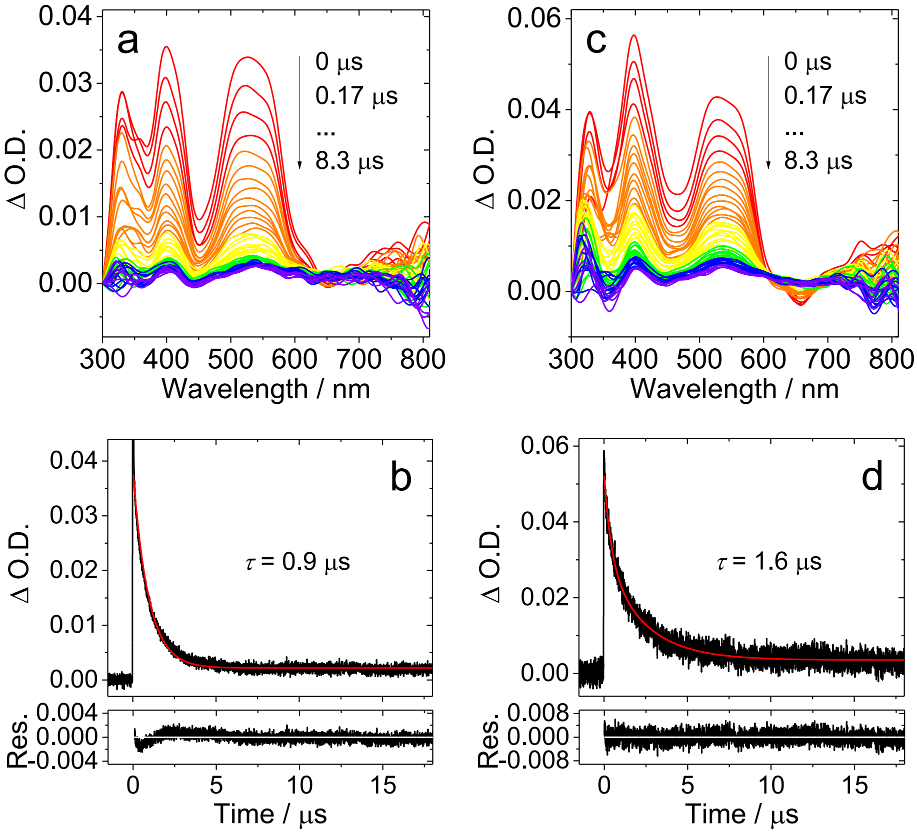

Figure S33. Nanosecond transient absorption spectra of (a) [Pt(**L**^{4})(acac)] and (c) [Pt(**L**^{5})(acac)] and the decay trace of (b) [Pt(**L**^{4})(acac)] and (d) [Pt(**L**^{5})(acac)] at 540 nm in *deaerated* toluene excited with nanosecond pulsed laser. λ_{ex} = 355 nm. c = 3.0 × 10^{-5} M, 25 °C.

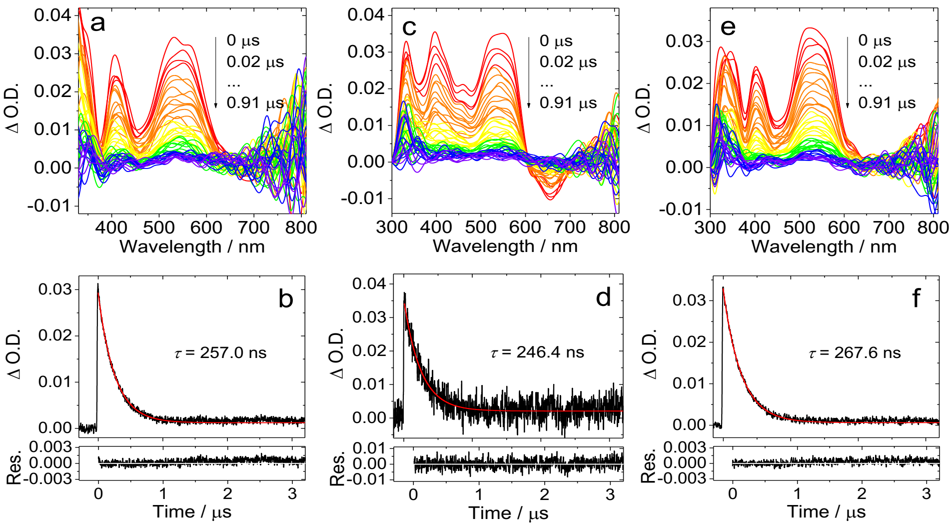

Figure S34. Nanosecond transient absorption spectra of (a) [Pt(**L**^{1})(acac)], (c) [Pt(**L**^{2})(acac)] and (e) [Pt(**L**^{3})(acac)] and the decay trace of (b) [Pt(**L**^{1})(acac)], (d) [Pt(**L**^{2})(acac)] and (f) [Pt(**L**^{3})(acac)] at 540 nm in aerated toluene excited with nanosecond pulsed laser. λ_{ex} = 355 nm. c = 3.0 × 10^{-5} M, 25 °C.

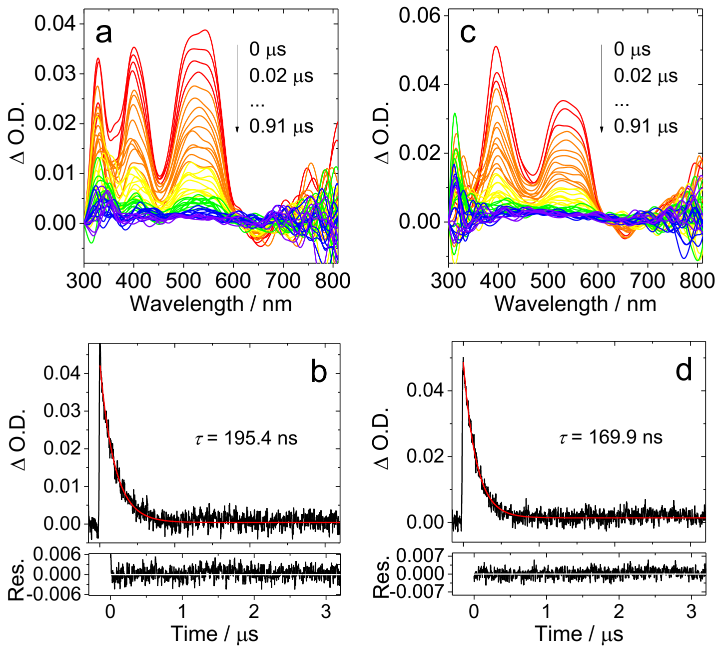

Figure S35. Nanosecond transient absorption spectra of (a) [Pt(**L**^{4})(acac)] and (c) [Pt(**L**^{5})(acac)] and the decay trace of (b) [Pt(**L**^{4})(acac)] and (d) [Pt(**L**^{5})(acac)] at 540 nm in aerated toluene excited with nanosecond pulsed laser. λ_{ex} = 355 nm. c = 3.0 × 10^{-5} M, 25 °C.

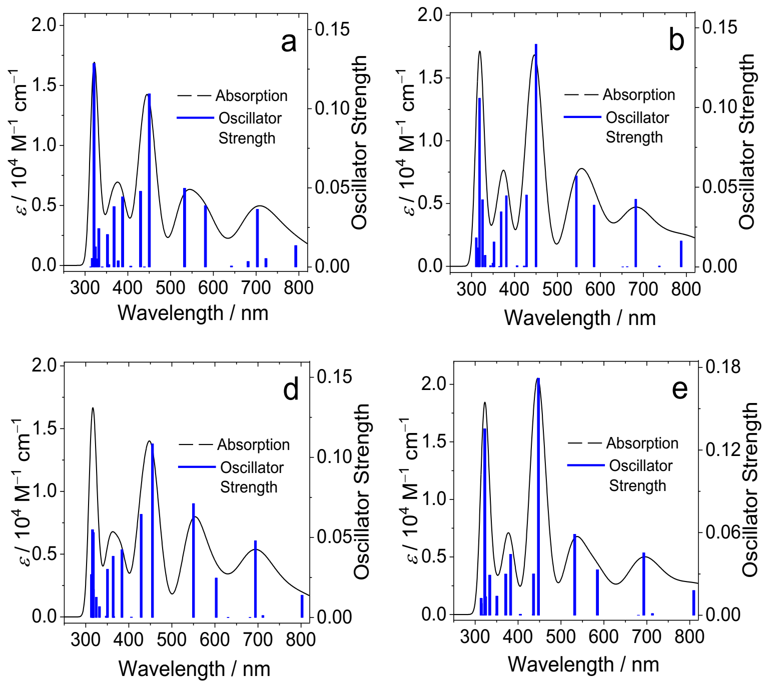

Figure S36. The calculated transient absorption spectra of (a) [Pt(**L1**)(acac)], (b) [Pt(**L2**)(acac)], (c) [Pt(**L3**)(acac)], (d) [Pt(**L4**)(acac)] and (e) [Pt(**L5**)(acac)], i.e. the $T_1 \rightarrow T_n$ transitions. The calculations were performed by TDDFT at the B3LYP/GENECP level in vacuum using Gaussian 09, based on the optimized triplet excited state (T_1) geometries performed by DFT at the B3LYP/GENECP level using Gaussian 09. The computation was performed under vacuum condition (no solvent was used for the computation).

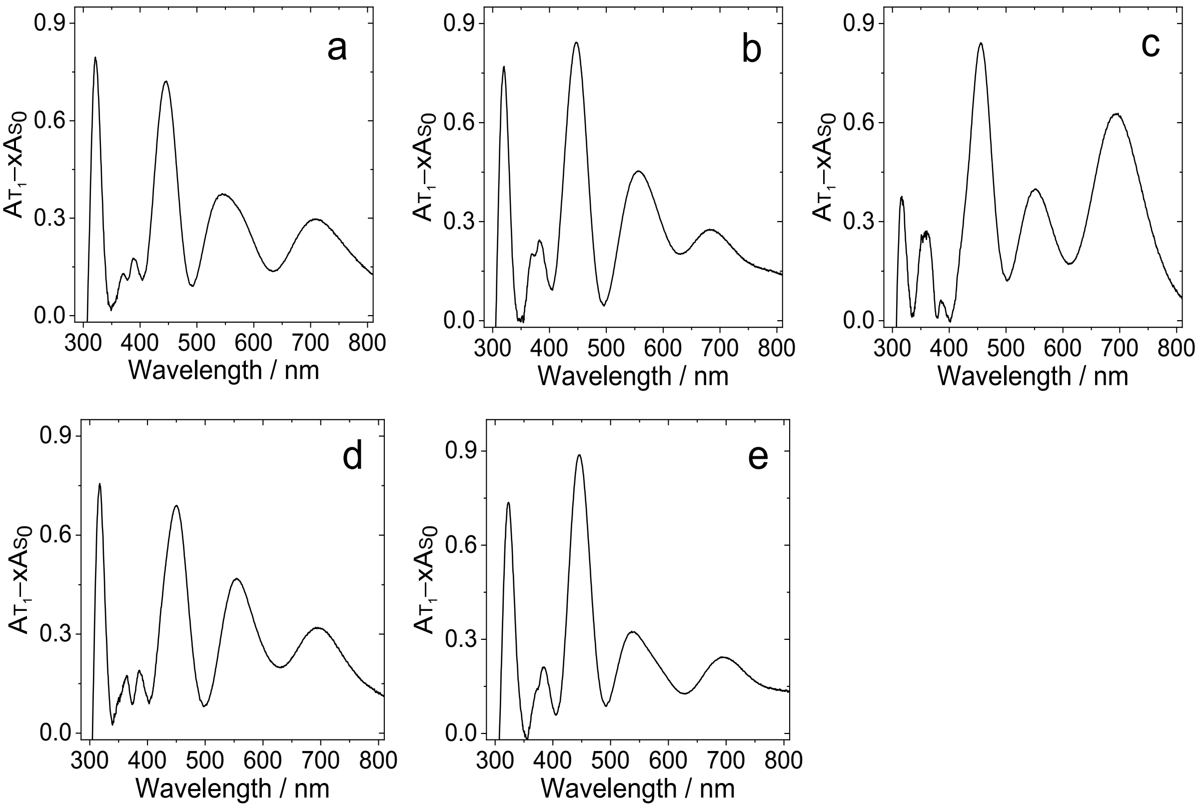

Figure S37. Absorbance differential spectrum of (a) [Pt(**L**[1])(acac)], (b) [Pt(**L**[2])(acac)], (c) [Pt(**L**[3])(acac)], (d) [Pt(**L**[4])(acac)] and (e) [Pt(**L**[5])(acac)], obtained by normalized transient absorption spectra minus a product of normalized UV-vis spectra and the coefficient (between 0~1), to simulate the nanosecond transient absorption spectra of the excited state absorption band overlapping the ground state band. The calculations for transient absorption are performed by TDDFT at the B3LYP/GENECP level in vacuum using Gaussian 09, based on the optimized triplet excited state geometries (performed by DFT at the B3LYP/GENECP level using Gaussian 09. In vacuum, no solvents were used).

Table S4. Electronic excitation energies (eV) and corresponding oscillator strengths (*f*) of the low-lying electronically excited states of the complexes. Performed by TDDFT at the B3LYP/GENECP level. No solvents were used in the calculations (under vacuum condition).

Compounds	Electronic transition	Energy (ev)	Wavelength (nm)	*f*
[Pt(**L**[1])(acac)]	$T_1 \rightarrow T_{10}$	1.7648	703	0.0365
	$T_1 \rightarrow T_{13}$	2.1340	581	0.0388
	$T_1 \rightarrow T_{14}$	2.3305	532	0.0498
	$T_1 \rightarrow T_{15}$	2.7574	450	0.1095
	$T_1 \rightarrow T_{17}$	2.8881	429	0.0479
	$T_1 \rightarrow T_{19}$	3.2019	387	0.0444
	$T_1 \rightarrow T_{28}$	3.8715	320	0.1286
[Pt(**L**[2])(acac)]	$T_1 \rightarrow T_{10}$	1.8180	682	0.0425
	$T_1 \rightarrow T_{14}$	2.2803	544	0.0571
	$T_1 \rightarrow T_{15}$	2.7572	450	0.1397
	$T_1 \rightarrow T_{16}$	2.8989	428	0.0451
	$T_1 \rightarrow T_{19}$	3.2581	381	0.0447
	$T_1 \rightarrow T_{28}$	3.8980	318	0.1059
[Pt(**L**[3])(acac)]	$T_1 \rightarrow T_{10}$	1.7918	692	0.0980
	$T_1 \rightarrow T_{14}$	2.2788	544	0.0541
	$T_1 \rightarrow T_{15}$	2.7107	457	0.1470
	$T_1 \rightarrow T_{16}$	2.9062	427	0.0551
	$T_1 \rightarrow T_{22}$	3.5124	353	0.0719
	$T_1 \rightarrow T_{28}$	3.9388	315	0.0853
[Pt(**L**[4])(acac)]	$T_1 \rightarrow T_{10}$	1.7866	694	0.0480
	$T_1 \rightarrow T_{14}$	2.2543	550	0.0712
	$T_1 \rightarrow T_{15}$	2.7276	455	0.1085
	$T_1 \rightarrow T_{17}$	2.8939	428	0.0424
	$T_1 \rightarrow T_{19}$	3.2305	384	0.0645
	$T_1 \rightarrow T_{28}$	3.9076	317	0.0531
	$T_1 \rightarrow T_{29}$	3.9316	315	0.0549
[Pt(**L**[5])(acac)]	$T_1 \rightarrow T_{10}$	1.7901	693	0.0454
	$T_1 \rightarrow T_{13}$	2.1210	585	0.0331
	$T_1 \rightarrow T_{14}$	2.3321	532	0.0588
	$T_1 \rightarrow T_{15}$	2.7726	447	0.1722
	$T_1 \rightarrow T_{20}$	3.3428	371	0.0300
	$T_1 \rightarrow T_{27}$	3.8495	322	0.1355

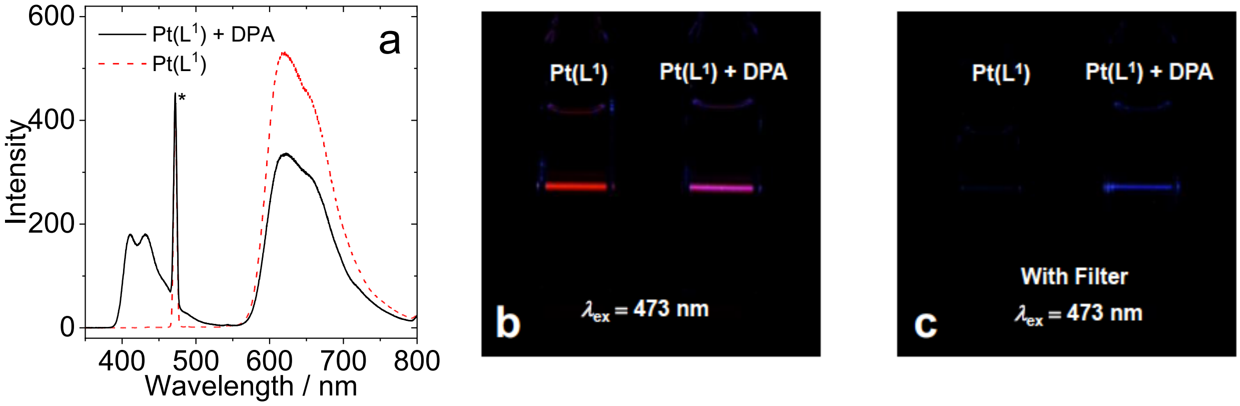

Figure S38. (a) TTA upconversion emission spectra with [Pt(**L**[1])(acac] as the photosensitizer and DPA as the acceptor in deaerated DCM. The asterisks indicate the scattered laser. (b) Photographs of [Pt(**L**[1])(acac] alone and the upconversion. (c) Photographs of upconversion solutions observed with band-pass filter (transparent in the range 380−520 nm). Excited with a 473 nm cw-laser with a power density of 80 mW cm^{-2}. $c_{[PSs]}$ = 1.0 × 10^{-5} M, $c_{[DPA]}$ = 3.0 × 10^{-5} M, 25 °C.

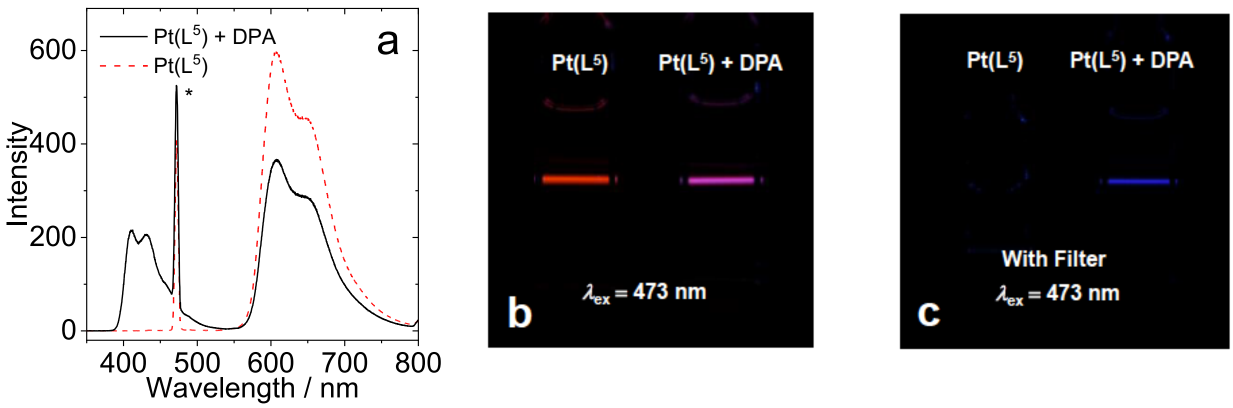

Figure S39. (a) TTA upconversion emission spectra with [Pt(**L**[5])(acac] as the photosensitizer and DPA as the acceptor in deaerated DCM. The asterisks indicate the scattered laser. (b) Photographs of [Pt(**L**[5])(acac] alone and the upconversion. (c) Photographs of upconversion solutions observed with band-pass filter (transparent in the range 380−520 nm). Excited with a 473 nm cw-laser with a power density of 80 mW cm^{-2}. $c_{[PSs]}$ = 1.0 × 10^{-5} M, $c_{[DPA]}$ = 3.0 × 10^{-5} M, 25 °C.